Experimental study of an organic Rankine cycle with R1233zd(E) for waste heat recovery from the coolant of a heavy-duty truck engine

Energy Conversion and Management 244 (2021) 114500

Contents lists available at ScienceDirect

Energy Conversion and Management

journal homepage: www.elsevier.com/locate/enconman

Experimental study of an organic Rankine cycle with R1233zd(E) for waste heat recovery from the coolant of a heavy-duty truck engine

Jelmer Rijpkema *, Sven B. Andersson, Karin Munch

Chalmers University of Technology, Gothenburg, Sweden

ARTICLE INFO

Keywords:
Engine coolant
Experiments
Heavy-duty Diesel
Internal combustion engine
Low-temperature
Long haul truck
Organic Rankine cycle (ORC)
R1233zd(E)
Vane expander
Waste heat recovery

ABSTRACT

Waste heat recovery is an effective method for improving engine efficiency. While most research on waste heat recovery from heavy-duty engines focuses on the high-temperature heat sources, this paper investigates the performance of a low-temperature system. The experimental setup features an organic Rankine cycle with R1233zd(E) as the working fluid recovering heat from the coolant of a heavy-duty Diesel engine. Experiments at multiple engine operating points indicated a maximum operating cycle pressure of 8 bar and temperature of 92 °C. Between 0.1 and 0.7 kW net shaft power was achieved with a thermodynamic efficiency between 1.1 and 1.8%, resulting in a maximum expander power of 0.7% relative to the engine power. A simple empirical model based on the experimental results indicated that approximately 0.7% of the engine's energy could be recovered during a driving cycle, rising to 1.3% if a high efficiency pump and expander are used. The main contribution of this paper lies in the presentation of the experimental setup and experimental results specifically dedicated to recovering the heat from the engine coolant, which permits realistic evaluation of the performance.

1. Introduction

Global concern over rising CO_2 emissions and their effects on climate change has led to regulations mandating emission reductions in all relevant sectors. A considerable fraction of the emissions in the transport sector originates from the burning of fossil fuels in engines of heavy-duty trucks [1]. Despite great ongoing efforts to reduce society's dependency on the internal combustion engine, it will retain an important role for the foreseeable future [2]. Therefore, improvements in engine efficiency are needed to reduce the impact of transport vehicles. Short-term solutions include increasing combustion efficiency, alternative fuels, loss reduction, electrification, and waste heat recovery (WHR) [3]. Among the available options for WHR, the organic Rankine cycle (ORC) is an attractive choice, due to its promising performance and relatively low complexity and costs [4]. Consequently, there have been numerous studies on the ORC, including working fluid selection [5], expander selection [6], cycle architectures [7], thermo-economical optimization [8], and dynamic modeling [9]. WHR systems for internal combustion engines typically target high-temperature (HT) heat sources (e.g. the exhaust gas recirculation (EGR) cooler and the exhaust gas) due to their high heat content and temperature, while low-temperature (LT) heat sources (e.g. the coolant, the charge air cooler (CAC), and the lubricant oil) are ignored because of their lower temperature and potential [4]. This paper focuses on waste heat recovery from the engine coolant of a heavy-duty Diesel engine. Although the temperature of the coolant is low, it contains a considerable amount of energy due to its high mass flow and specific heat, even exceeding the exhaust gas energy under low speed, high load operating conditions [10,11]. An opportunity to enhance the quality of the energy of the engine coolant is to raise its temperature, which could improve the performance of WHR systems or allow the use of higher condensation temperatures without reducing system performance. While raising the coolant temperature could adversely affect engine performance, coolant temperatures as high as 140 °C did not significantly impact the engine efficiency in experimental studies [12].

The selection of a suitable working fluid for low-temperature WHR has been extensively discussed in literature [13,14,5,15]. The optimal choice depends heavily on the operating conditions of the heat source, the chosen boundary conditions and limitations, and whether packaging, economic issues, and environmental impact are taken into account. Popular choices include alkanes, alcohols, siloxanes, and, especially for low-temperature WHR, refrigerants [13]. Refrigerants are typically non-flammable and non-toxic, but their environmental effects in terms of global warming potential (GWP) and ozone depletion potential (ODP) might be of concern. In previous studies [16–19], R245fa

* Corresponding author.
E-mail address: jelmer.rijpkema@chalmers.se (J. Rijpkema).

https://doi.org/10.1016/j.enconman.2021.114500
Received 4 March 2021; Accepted 4 July 2021
Available online 21 July 2021

Nomenclature

h	specific enthalpy (J/kg)
$\dot{m}$	mass flow rate (kg/s)
N	rotational speed (rpm)
p	pressure (Pa)
Q	heat transfer (J)
$\dot{Q}$	heat transfer rate (W)
r_p	pressure ratio (–)
T	temperature (K)
V	volume (m^3)
$\dot{V}$	volume flow (m^3/s)
$\dot{W}$	power (W)
W	work (J)

Greek symbols

ϵ	effectiveness (–)
η	efficiency (–)
ρ	density (kg/m^3)
τ	torque (Nm)
ϕ_f	filling factor (–)

Subscripts

cond	condenser
cool	coolant
el	electrical
eng	engine
evap	evaporator
exh	exhaust
exp	expander
mech	mechanical
pmp	pump
is	isentropic
sh	shaft
sub	subcooling
sup	superheating
th	thermodynamic

Abbreviations

BPV	bypass valve
CAC	charge air cooler
EGR	exhaust gas recirculation
ESC	European stationary cycle
HT	high-temperature
LT	low-temperature
ORC	organic Rankine cycle
TS	thermostat
SV	safety valve
WHR	waste heat recovery

was identified as a particularly favorable refrigerant for WHR from engines because of its thermodynamic potential. However, it is disfavored nowadays due to its high GWP value of 858. Recent studies [20,21] have shown that R1233zd(E) is a low GWP alternative with similar thermophysical properties, making it an environmentally friendly alternative to R245fa. A previous simulation study by the authors [22], taking into account a large selection of working fluids, has also shown that R1233zd (E) gives good thermodynamic performance for WHR in heavy-duty engines. For this reason, R1233zd(E) was chosen as the working fluid for the experimental study presented in this paper.

There have been relatively few published studies in which the engine coolant was investigated as the sole heat source for WHR in a heavy-duty truck engine; the coolant is more commonly investigated as part of a combined system that uses multiple heat sources from the engine. Several studies are listed in Table 1. Peris et al. [23] focused on recovering heat from the coolant using different architectures and working fluids and found that SES36 was the best performing fluid, achieving a net electrical efficiency of 7.15%. Rijpkema et al. [22] evaluated the performance of four thermodynamic cycles for HT and LT sources in a heavy-duty engine and found that the highest net power (1.8 kW) at a 100 kW engine operating point was achieved using the ORC with isohexane, acetone, or cyclopentane. Mashadi et al. [24] investigated the use of 19 working fluids for coolant heat recovery in a light-duty Diesel engine and found that the maximum net power of 5.0 kW (7.9% of the engine's power) was achieved with ammonia. In a system with multiple heat sources, single-loop configurations use a conventional ORC with multiple heat exchangers, which may be combined in series, parallel, or both. In dual-loop configurations, the heat rejected during condensation in the HT loop is used to evaporate the fluid in the LT loop, allowing each loop to use a different working fluid in order to maximize performance. In combined-loop configurations, the HT and LT loops use the same fluid and the expander outlet of the HT loop is connected to the expander inlet

Table 1
Selected publications on waste heat recovery from heavy-duty engine coolant.

Reference	Year	Study	Heat source(s)	Fluids(s)*	$\dot{W}_{max}$	$\dot{W}_{max}$
-	-	-	-	-	kW	%
Peris et al. [23]	2013	Simulations	Coolant	SES36	-	7.2
Yu et al. [18]	2013	Simulations	Coolant + Exhaust	R245fa	15.5	6.0
Furukawa et al. [25]	2014	Experiments	Coolant + Exhaust + EGR	HFE	-	7.5
Yang et al. [19]	2014	Simulations	CAC + Coolant + Exhaust	R245fa	27.9	11
Shu et al. [26]	2016	Simulations	CAC + Coolant + EGR + Exhaust	Toluene + R143a	33.9	14
Chen et al. [27]	2017	Simulations	Coolant + Exhaust	Cyclopentane	29.0	9.5
Liu et al. [28]	2018	Simulations	Coolant + EGR Exhaust	Cyclohexane	21.3	9.0
Rijpkema et al. [22]	2018	Simulations	Coolant	Isohexane	1.8	1.8
Rijpkema et al. [29]	2019	Simulations	CAC + Coolant + EGR + Exhaust	Acetone, Cyclopentane	6.5	6.5
Mashadi et al. [24]	2019	Simulations	Coolant	Ammonia	5.0	7.9
Thantla et al. [30]	2019	Simulations	Coolant + Exhaust	R1233zd(E)	7.0	5.5
Singh et al. [12]	2020	Simulations	Coolant + Exhaust	Cyclopentane + Methanol	14.0	9.0

*Best performing working fluid(s).

of the LT loop; consequently, only one condenser is necessary. Yu et al. [18] studied the effect of preheating R245fa with the engine coolant before evaporating it using thermal oil heated by the exhaust gas. Their simulations indicated a maximum expander power of 15.5 kW, corresponding to a relative power of 6.0%. In their experimental study, Furukawa et al. [25] recovered heat from the exhaust gases, the EGR, and the engine coolant using a single-loop in series, resulting in a 7.5% reduction in fuel consumption. Yang et al. [19] simulated a dual-loop configuration with R245fa in a HT loop using the exhaust gases and a LT loop using the CAC, HT condenser, and the engine coolant. This system achieved a power output of 10.0 kW for the HT loop and 17.9 kW for LT loop, resulting in a combined relative power of 11%. Shu et al. [26] reported simulations of a dual-loop configuration with eight different working fluid using a combination of the CAC, the coolant, the EGR, and the exhaust gases. This system performed optimally with toluene in the HT loop and R143a in the LT loop, delivering a maximum power output of 33.9 kw (14%). Chen et al. [27] simulated dual- and combined-loop configurations with six different working fluids and found that the combined-loop with cyclopentane gave the best performance with a net power of 29.0 kW and a relative power of 9.48%. Liu et al. [28] examined eight alkanes in a single-loop series configuration with two-stage expansion. Cyclohexane offered the best performance, achieving absolute and relative power outputs of 21.3 kW and 9.0%, respectively. Rijpkema et al. [29] investigated fifty working fluids in four different thermodynamic cycles using the CAC, engine coolant, EGR, and exhaust gases as the heat sources. Two single-loop series configurations were simulated, one with and one without the engine coolant. In this study, a maximum net power of 6.5 kW at a 100 kW engine operating point was obtained using the ORC with acetone, cyclopentane, ethanol, or methanol as the working fluid. Thantla et al. [30] used simulations to predict the performance of a combined-loop configuration with R1233zd(E) using the exhaust gases and engine coolant and achieved a maximum power output of 7 kW, leading to fuel savings of 5.5%. Singh et al. [12] combined cycle simulations and engine experiments to study the effect of elevated coolant temperatures in a dual-loop configuration using ten working fluids, with the exhaust gases and coolant as heat sources. The best results were obtained with methanol in the HT loop and cyclopentane in the LT loop, delivering 10.5 and 3.5 kW, respectively, leading to a potential fuel consumption reduction up to 9% over a driving cycle. Although, for performance reasons, it makes sense to include HT sources for engine WHR, a dedicated coolant heat recovery system has some distinct advantages. First, there is no heat load added to the system. Of course, this has the disadvantage that heat is rejected at a lower temperature, but the adverse impact is reduced by improved heat transfer characteristics during condensation. Second, although low pressures and temperatures are detrimental to thermodynamic performance, they could be beneficial from a mechanical and economical perspective. Finally, such systems are less complex than multiple loop systems even though they require an extra radiator.

This paper presents an experimental evaluation of the performance of a LT-WHR system and uses the experimental results to develop a simple empirical model to evaluate the system performance over a driving cycle. Experimental studies presenting detailed empirical results on waste heat recovery from heavy-duty engine coolant are very scarce. Therefore, the main contribution of this paper is the presentation of the experimental setup and results of an ORC coupled to a heavy-duty engine using R1233zd(E) as the working fluid. Not only can this serve as a useful reference for further simulation studies, the experimental results were also used to develop a simple empirical model to give a realistic evaluation of such a system in a long haul driving cycle.

2. Experimental Setup

This section provides an overview of the system components and sensors. Fig. 1 and 2 show the test cell containing the experimental setup of the low-temperature waste heat recovery (LT-WHR) system and the heavy duty Diesel engine with the corresponding schematic overview and locations of the sensors shown in Fig. 3. The specifications of the components are summarized in Table 2 and the measurement accuracies of the sensors are listed in Table 3. More detailed information on each of the main components (engine, pump, evaporator, expander, and condenser) is given in the Experimental Results 3 section.

The engine is a 12.8 L Volvo heavy-duty Diesel engine used in long haul trucks. The engine coolant which is used as the heat source for the WHR system, is a 50/50 volumetric mixture of water/ethylene–glycol. The coolant pump is connected to the crankshaft of the engine. Therefore, the engine speed controls the pump speed and thereby the coolant volume flow. Some of the coolant is recirculated in the engine and part is directed to the radiator. The flow to the radiator is controlled using the engine thermostat, which starts opening at 82 °C and is fully open at 92 °C. In the test cell, the radiator is replaced with a plate heat exchanger cooled by the available process water. The engine coolant

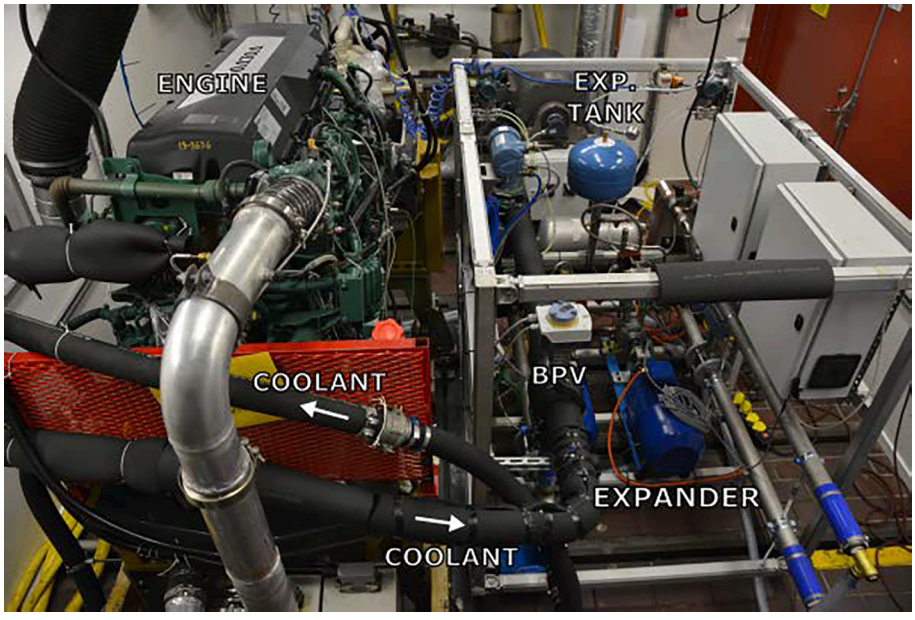

Fig. 1. Heavy-duty engine connected to the LT-WHR setup.

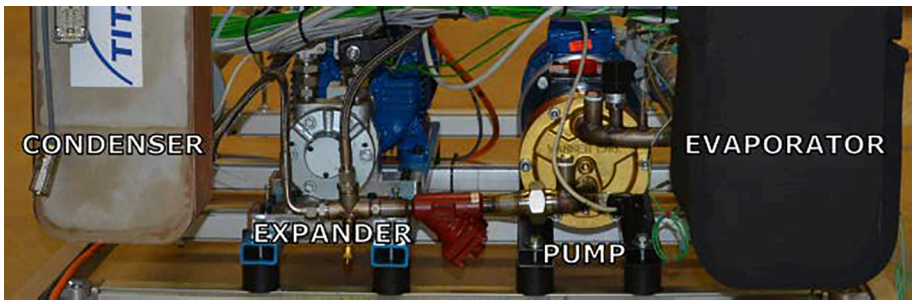

Fig. 2. LT-WHR pump, expander, and heat exchangers.

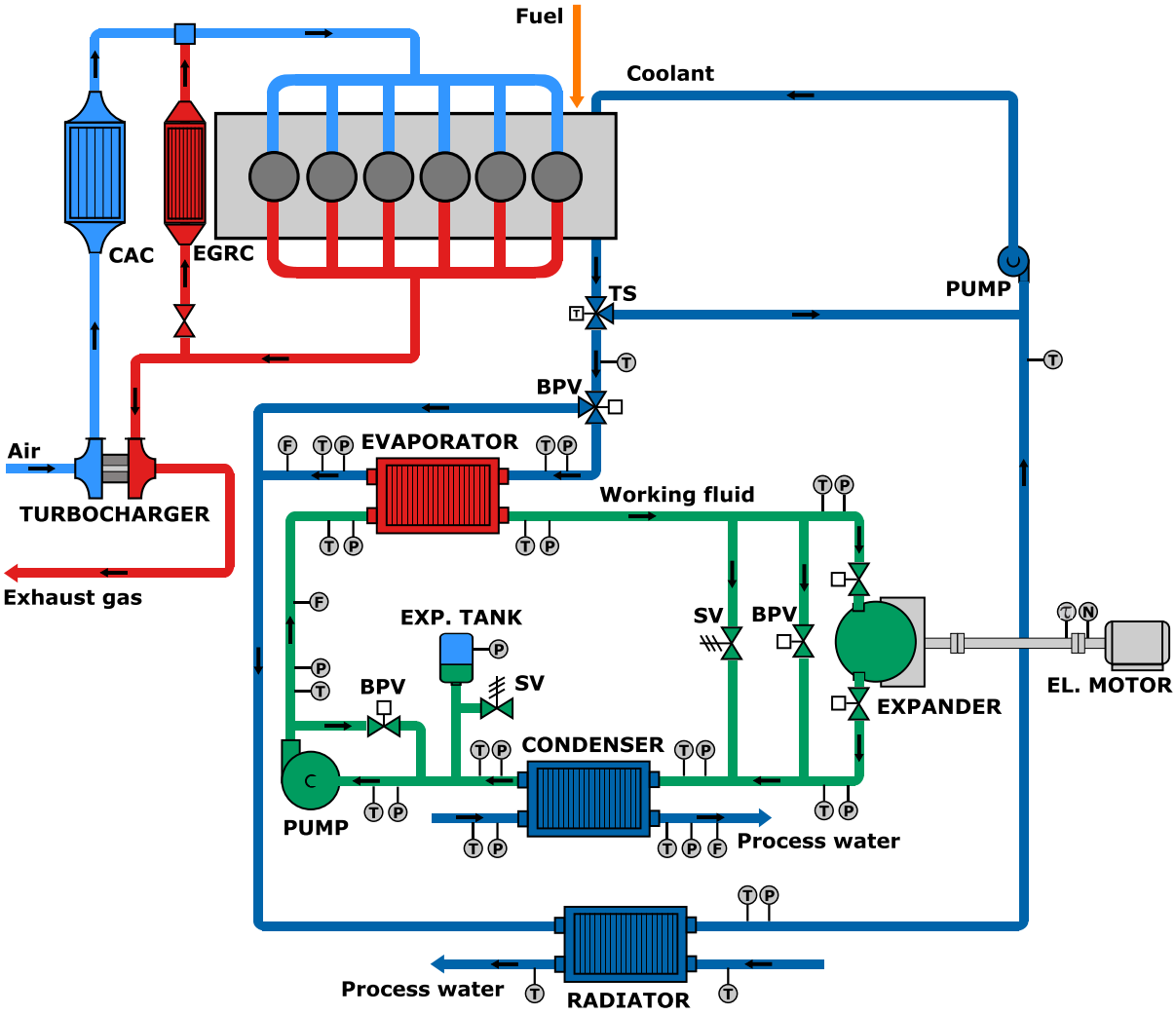

Fig. 3. Schematic depiction of the experimental setup and sensors.

outlet is connected to the evaporator inlet with insulated hoses and a 3-way bypass valve (BPV) is installed between the coolant outlet and evaporator inlet to control the flow of coolant to the WHR system and the radiator. Typically, during start-up, the coolant bypass valve is only open to the radiator, allowing the engine to heat up. When the engine reaches its desired temperature, the coolant valve is fully opened to the WHR system, so that no flow is bypassed and all flow passes through the WHR system.

The WHR system is an organic Rankine cycle with R1233zd(E) as the working fluid containing 5% (mass) Emkarate RL 32-3MAF refrigeration lubricant. Its pressure is regulated using an 12 L expansion tank with a membrane. On one side of the membrane the air pressure is controlled using a pressure regulator that takes compressed air from the test cell and sets the condensation pressure for the working fluid on the other side. A low-pressure safety valve is installed that vents directly into the test cell in case the condensation pressure exceeds 8 bar(g). Working fluid leaving the expansion tank enters the diaphragm pump, which raises its pressure. As shown in Fig. 3, the system is fitted with a pump bypass valve that allows the flow to the evaporator to be reduced even when the pump is operating at its minimum speed. Although the pump bypass valve was installed on the system, it was not used during the experiments reported in this paper. From the pump, the working fluid

Table 2
Cycle component specifications.

Component	Brand	Type	Controller
Coolant bypass valve	Siemens VXG41	3-Port seat valve	Siemens SAX61
Expansion tank	Armatec AT 8321E12	Diaphragm	
Air pressure regulator	SMC ITV1050	Electro-pneumatic	
Pump	Wanner-Hydracell G10	Seal-less diaphragm pump	
Pump bypass valve	Swagelok SS-18RS12MM	Integral-bonnet needle	Hanbay MCL-000AF
Pump electric motor	BEVI IE3 90–4-150	250 V, 1450 rpm, 1.5 kW	IMO iDrive EDX-220–21-E
Evaporator	SWEP B250ASHx100	Plate, counter-current	
Expander	GAST 6AM-FRV-5A	Sliding vane, 4 vanes	
Expander bypass valve	Swagelok SS-18RS18MM	Integral-bonnet needle	Hanbay MCL-000AF
Expander inlet valves	Bürkert 22192	Solenoid valve	
Expander electric motor	BEVI IE3 3SIE 112-M2	400 V, 2920 rpm, 4.8 kW	Delta C2000
Condenser	SWEP B250ASHx60	Plate, counter-current	
High pressure safety valve	Swagelok SS-R4S12MM	Proportional relief valve	
Low pressure safety valve	Swagelok SS-RL4S12MM	Proportional relief valve	
In-line filters	Danfoss 148B5243	Strainer	

Table 3
Accuracy of measurement devices.

Input	Type	Range	Accuracy	Unit
Engine speed	Schenck D900-1e	0– 6500	± 2	rpm
Engine torque	Schenck D900-1e	−4000–4000	± 8	Nm
Expander speed	HBM T22	0–3000	± 15	rpm
Expander torque	HBM T22	−100–100	± 0.5	Nm
Cycle flow	Micro Motion F025S	0–600	± 3.0	g/s
Engine coolant flow	Rosemount 8800A	0–10	± 0.07	L/s
Cycle high pressure	WIKA A-10	0–10	± 0.05	bar (g)
Cycle low pressure	WIKA A-10	0–6	± 0.03	bar (g)
Air pressure	WIKA A-10	0–9	± 0.05	bar (g)
Engine coolant pressure	WIKA A-10	0–4	± 0.02	bar (g)
Temperature	RS Pro Type K	−75–1100	± 1.5	°C

enters the evaporator (a counter-current plate heat exchanger) in which the heat is transferred from the engine coolant to the working fluid. Before entering the slide vane expander, the fluid must be superheated sufficiently to ensure vapor conditions at the inlet of the expander. If this is not the case (e.g. during start-up), the expander inlet and outlet valves are closed and the expander bypass valve is left open until sufficient superheating is achieved. When sufficiently superheated, the expander bypass valve is closed, the expander inlet and outlet valves are opened, and the expander speed is set using the connected electric motor. Additionally, a high-pressure safety valve is installed which is set to open if the evaporation pressure exceeds 12 bar(g). At the expander outlet, the working fluid is still in the vapor phase, but at a low pressure. From there it enters the condenser (another counter-current plate heat exchanger), where the fluid is condensed and subcooled using the process water from the test cell. The process water flow and temperature are not controlled, meaning that the condenser outlet temperature is similar to the process water temperature, which varies between 10 and 20 °C. Since the system is typically operated at a condensation pressure of 3 bar (≈ 50 °C), the working fluid is sufficiently subcooled before entering the pump.

The engine is connected to a Schenck D900-1e water brake with its own control unit, which is used to set the engine speed. The engine torque is controlled using the standard gas pedal of a truck which is mounted in the control room adjacent to the test cell. The measurements for the engine are collected with a NI CompactRIO 9074 chassis containing modules for acquisition of temperature, analog, and digital sensor readings. Using a Labview interface, the data is converted to physical signals and stored. The LT-WHR system has its own stand-alone data acquisition and control system with another NI CompactRIO 9074 chassis connected to a separate Labview interface. MATLAB [31] and CoolProp [32] are used for post-processing and evaluation of the data.

3. Experimental results

This section presents the experimental results of the main components in the WHR system: the engine, the pump, the evaporator, the expander, and the condenser. To evaluate the cycle performance, the absolute and relative power output as well as the thermodynamic efficiency are reported. In addition, experimental results containing the influence of the engine coolant temperature and the condensation pressure on the performance are presented. The maximum errors of the derived physical quantities (i.e. the quantities not measured directly) are calculated using the general rule for error propagation [33] shown in Eq. (1). The resulting values are presented in Table 4 together with the corresponding symbols and expressions. The errors for the expander shaft power and its derived quantities are relatively large because the measured expander torque values were low compared to the range of the torque sensor.

$$\delta y = \sqrt{\sum_i \left(\frac{\partial y}{\partial x_i}\delta x_i\right)^2} \tag{1}$$

3.1. Engine

The heat for the LT-WHR system is provided by the engine coolant of a Volvo D13K540 heavy-duty Diesel engine, whose specifications are shown in Table 5. The coolant is a mixture of ethylene–glycol and water in an approximate volumetric ratio of 1:1.

The WHR system was evaluated at nine different engine operating points from the European Stationary Cycle (ESC) [34], named according to the ESC classification: the letters A, B, and C represent different engine speeds and the numbers 25, 50, and 75 indicate the percentage of the maximum torque available at that engine speed. Contour maps of the coolant mass flow ($\dot{m}_{cool}$) and the coolant temperature leaving the engine ($T_{cool,out}$) are shown in Fig. 4. At the 25% load points the thermostat is not fully open, restricting the flow. At the higher load points, the thermostat is fully open. Since the coolant pump is mechanically coupled to the engine, the mass flows at the higher load points are almost equal, except for small differences in density.

The corresponding heat transfer rate from the engine to the coolant ($\dot{Q}_{cool}$) is shown in Fig. 5, which is calculated from the mass flow ($\dot{m}_{cool}$) and the enthalpies at the inlet ($h_{cool,in}$) and outlet ($h_{cool,out}$) of the engine. The values from the figure can be interpreted as the maximum energy in the engine coolant available for waste heat recovery at the corresponding engine operating point.

3.2. Pump

The specifications of the pump, shown in Table 6, are taken from the manufacturer's data sheet [35]. The efficiencies of this pump at various pressures were determined in an earlier study [7] and were used here

Table 4
Maximum errors and equations for the derived quantities.

Quantity	Max. Error	Symbol	Equation	
Engine power	± 1.50 %	$\dot{W}_{eng}$	$2\pi\tau_{eng}N_{eng}/60$	(2)
Engine coolant mass flow	± 6.55 %	$\dot{m}_{cool}$	$\rho_{cool,out}\dot{V}_{cool,out}$	(3)
Engine coolant heat transfer rate	± 6.56 %	$\dot{Q}_{cool}$	$\dot{m}_{cool}(h_{cool,out} - h_{cool,in})$	(4)
Pump shaft power	± 3.25 %	$\dot{W}_{pmp}$	$\dot{m}_{pmp}(h_{pmp,out} - h_{pmp,in})/\eta_{pmp}$	(5)
Evaporator heat transfer rate	± 3.18 %	$\dot{Q}_{evap}$	$\dot{m}_{pmp}(h_{evap,out} - h_{evap,in})$	(6)
Expander shaft power	± 18.8 %	$\dot{W}_{exp}$	$2\pi\tau_{exp}N_{exp}/60$	(7)
Filling factor	± 3.98 %	ϕ_f	$\dot{m}_{pmp}/(\rho_{exp,in}V_{exp}N_{exp}/60)$	(8)
Expander efficiency	± 19.1 %	η_{exp}	$\dot{W}_{exp}/(\dot{m}_{pmp}[h_{exp,in} - h_{exp,out,is}])$	(9)
Expander isentropic effectiveness	± 0.55 %	$\epsilon_{is,exp}$	$(h_{exp,out} - h_{exp,in})/(h_{exp,out,is} - h_{exp,in})$	(10)
Condenser heat transfer rate	± 3.18 %	$\dot{Q}_{cond}$	$\dot{m}_{pmp}(h_{cond,in} - h_{cond,out})$	(11)
Cycle net power	± 19.1 %	$\dot{W}_{net}$	$\dot{W}_{exp} - \dot{W}_{pmp}$	(12)
Cycle thermodynamic efficiency	± 19.4 %	η_{th}	$\dot{W}_{net}/\dot{Q}_{evap}$	(13)

Table 5
Engine specifications.

Type	Volvo D13K540, EU6SCR
Configuration	4 Stroke/ 6 Cylinder inline/ EGR
Peak power	397 kW (540 hp)
Peak torque	2600 Nm
Compression ratio	17.0:1
Bore x Stroke	131 x 158 mm
Displacement	12.8 L

estimate its efficiency as a function of the pressure differential over the pump.

Diaphragm pumps are insensitive to pressure, meaning that the mass flow ($\dot{m}_{pmp}$) depends mainly on the pump speed (N_{pmp}), as shown on the left of Fig. 6. The figure also shows that the pump speed did not exceed 450 rpm during the experiments even though the maximum speed is 1450 rpm. This was due to the large fluctuations in the pump inlet pressure at higher pump speeds. The corresponding power output ($\dot{W}_{pmp}$) is presented on the right of Fig. 6 and was calculated by dividing the energy added to the flow by the estimated efficiency, as shown in Eq. (5) in Table 4. The variation in pump power at each pump speed corresponds to the variation in pump outlet pressure.

3.3. Evaporator

The evaporator was selected based on design software from the manufacturer [36]; its specifications are shown in Table 7. Using the software, the heat exchanger was sized for the estimated maximum heat load during the experiments while minimizing the pressure drop.

The evaporator heat transfer rate ($\dot{Q}_{evap}$) is shown on the left of Fig. 7. A comparison of this heat transfer rate to the available coolant energy ($\dot{Q}_{cool}$) in Fig. 5 suggests that only a fraction of the available coolant energy was transferred to the working fluid. This is shown clearly on the right of Fig. 7, where the evaporator heat transfer rate is divided by the available coolant energy, revealing that only between 10 and 60% of the available heat was recovered. There are two main reasons for this. First, due to the limitations on the pump speed, the mass flow in the cycle was insufficient to extract all the available heat from the engine coolant. Second, part of the available heat from the engine coolant was lost between the engine outlet and evaporator inlet.

3.4. Expander

The expander is an air motor whose vanes and shaft seal were replaced to withstand higher temperatures and pressures. The specifications of the expander are based on the data supplied by the manufacturer [37] and previous geometrical measurements [38]. These measurements were used to estimate the displaced volume with the following equation [39]:

$$V_{exp} = 2eL(\pi D - ms) \quad (2)$$

The mass flow in the system was controlled by the pump speed (N_{pmp}), the pressure by the expander speed (N_{exp}), and the heat input depended on the engine operating point. Both the pump and expander speed were varied at each of the nine engine operating points

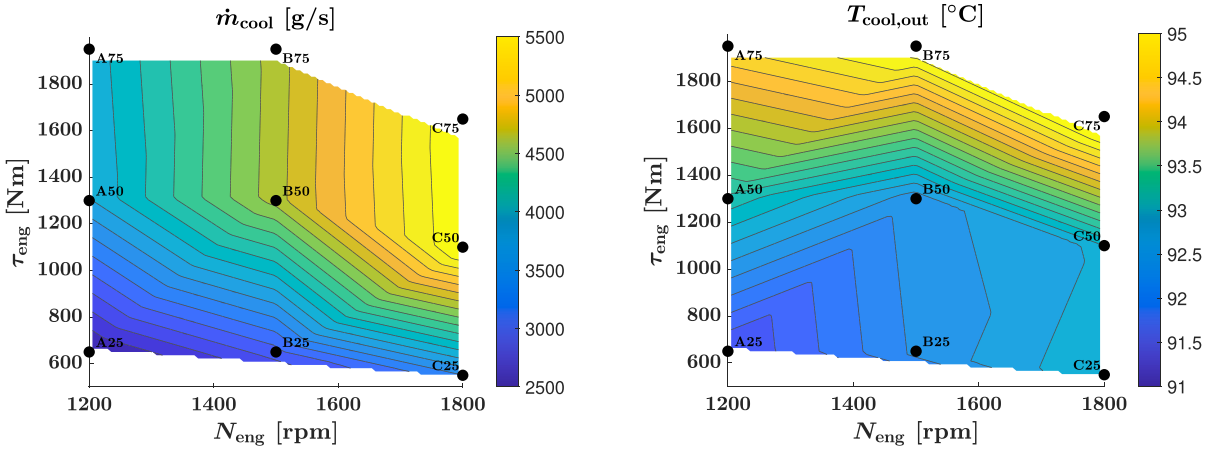

Fig. 4. Engine speed-torque map showing the engine coolant mass flow (left) and outlet temperature (right).

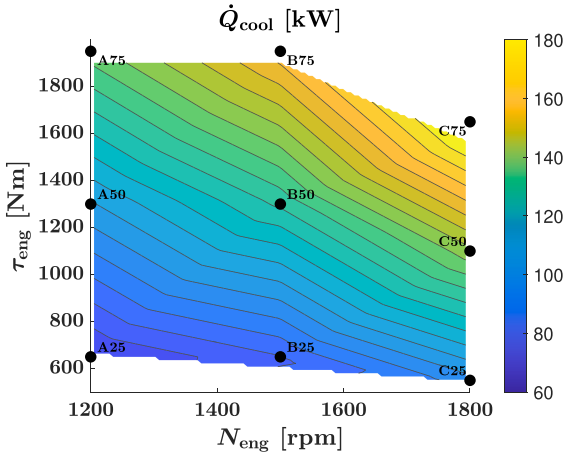

Fig. 5. Engine speed-torque map showing the engine coolant heat transfer rate.

Table 6
Pump specifications [35].

Brand	Wanner-Hydracell G10-X	
Type	Seal-less diaphragm pump	
Displacement	V_{pmp}	0.023 L
Max. speed	N_{pmp}	1450 rpm
Max. volume flow	$\dot{V}_{pmp}$	33.4 L/min
Efficiency [7]	η_{pmp}	0.24–0.40

(A25–C75), which is shown in Fig. 8. Neither the pump nor the expander were operated at their maximum speed because they were limited by pressure fluctuations in the system. The expander inlet temperature ($T_{exp,in}$) and pressure ($p_{exp,in}$) are shown in Fig. 9 and 10. Because in most cases the cycle mass flow was not limited by the available heat in the engine coolant, the expander inlet temperature was close to the engine coolant temperature at the inlet of the evaporator. The inlet pressure was determined by the interaction between the pump and expander: a high pump speed and a low expander speed led to a high system pressure, and vice versa. Fig. 11 shows the resulting expander shaft power, calculated from the expander torque and speed measurements using Eq. (7) in Table 4. The maximum shaft power output of the expander was around 1.2 kW at an expander pressure ratio of 2.2. The performance of the expander can also be characterized by comparing it to the theoretical performance using the filling factor (ϕ_f) and the efficiency (η_{exp}). These quantities are defined in Eq. (8) and (9), respectively, and their variation with the expander pressure ratio is shown in Fig. 12.Table 8.

3.5. Condenser

The condenser was selected using design software supplied by the manufacturer [36] and had the specifications shown in Table 9. Using the software, the heat exchanger was sized for the estimated maximum heat load during the experiments while minimizing the pressure drop.

In all of the experiments discussed in this section, the condensation pressure was kept at 3 bar, which corresponds to a condensation temperature of around 50 °C. The heat rejected from the cycle in the condenser ($\dot{Q}_{cond}$) is shown in Fig. 13. As expected, the condenser heat transfer rate was less than the evaporator heat transfer rate due to heat losses and power extracted by the expander. Because of the low temperature in the cycle, the heat loss and extracted power were relatively low, meaning that almost all heat transferred to the cycle was rejected in the condenser.

3.6. Cycle

The performance of the LT-WHR system was evaluated using the net (shaft) power of the cycle ($\dot{W}_{net}$) and the thermodynamic efficiency (η_{th}), which are defined in Eq. (12) and (13) and shown in Fig. 14. The net power is the expander power minus the pump power and its maximum was close to 0.7 kW. It is important to note the pump's significant power consumption, which ranged from 33 to 93% relative to the expander power. Due to the high energy content but low temperature of the heat source, the mass flow in the WHR system had to be large to extract this energy, leading to a high pump power. The thermodynamic efficiency, which indicates how well the extracted heat is converted to net power, reached a maximum of 1.8% for the system under investigation in this paper.

The objective of a WHR system is to maximize its power output using the available waste heat. The engine operating conditions (and corresponding power output) of heavy-duty engines change constantly during real world use, so the cycle performance should also be evaluated relative to the engine power. In the studied system, fluctuations in the pump and expander inlet pressure limited the pump and expander speed, preventing the system from extracting all the available heat. This is shown in Fig. 15, where the net power relative to the engine power

Table 7
Evaporator specifications [36].

Brand	SWEP B250ASHx100	
Type	Plate, counter-current	
Max. pressure drop	Δp_{evap}	3.70 kPa
Max. heat load	$\dot{Q}_{evap}$	125 kW

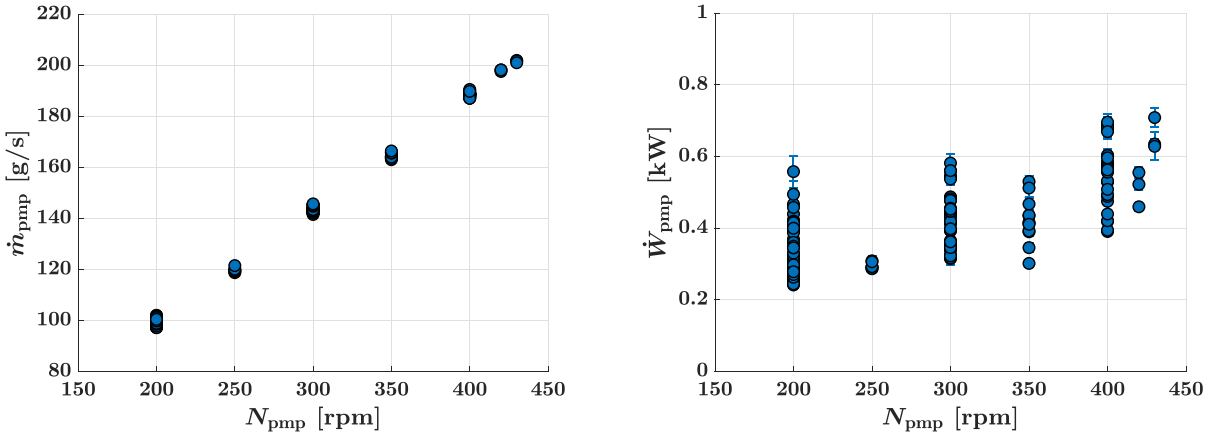

Fig. 6. Pump mass flow (left) and shaft power (right) as functions of the pump speed.

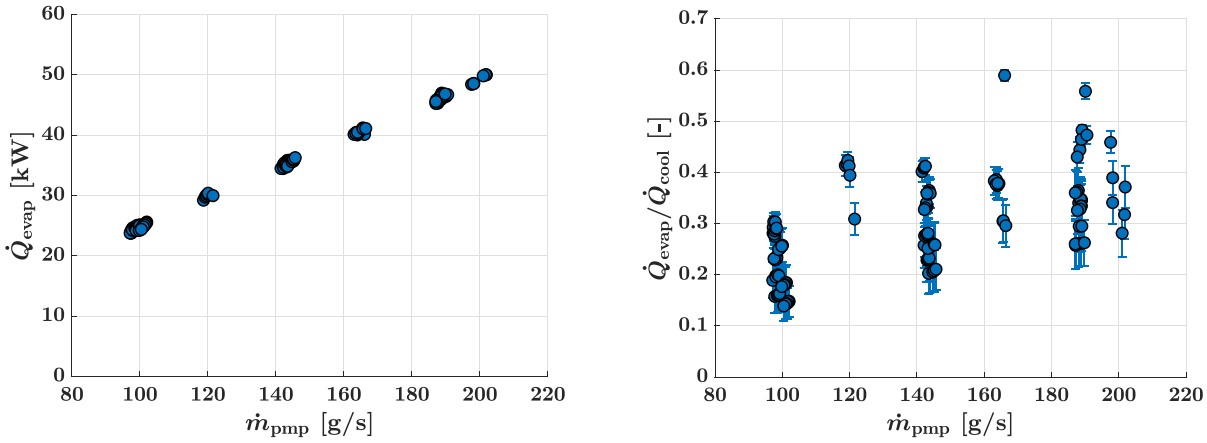

Fig. 7. Absolute (left) and relative (right) evaporator heat transfer rate as a function of the mass flow.

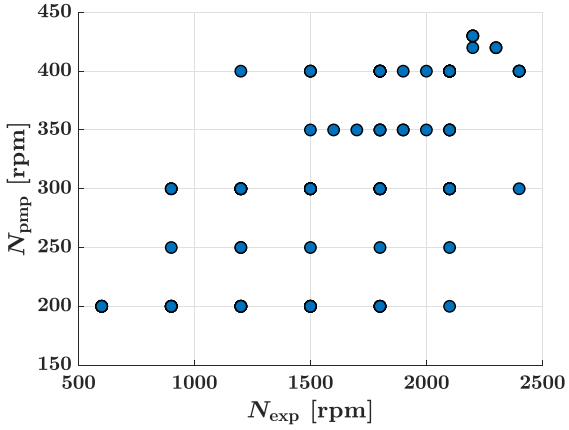

Fig. 8. Pump speed and expander speed.

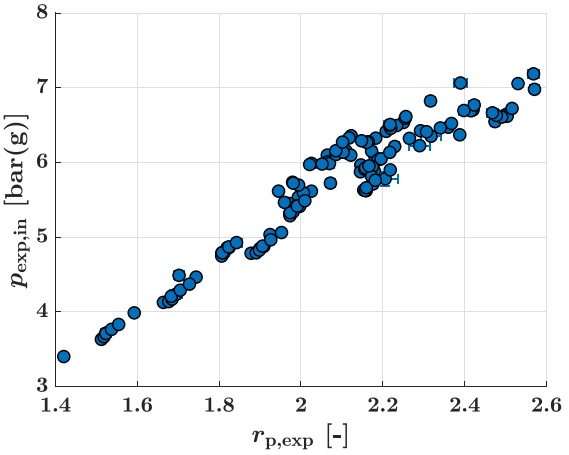

Fig. 10. Expander inlet pressure as a function of the expander pressure ratio.

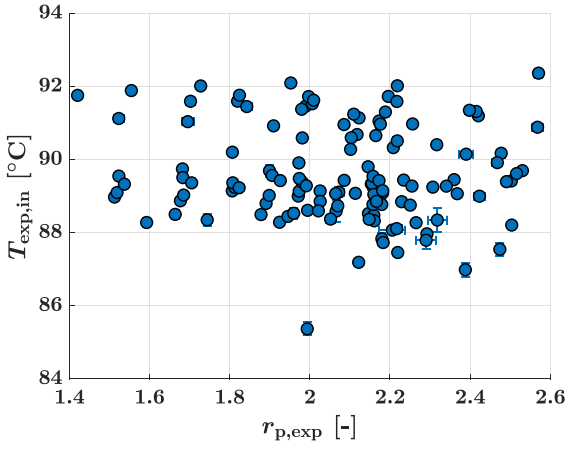

Fig. 9. Expander inlet temperature as a function of the expander pressure ratio.

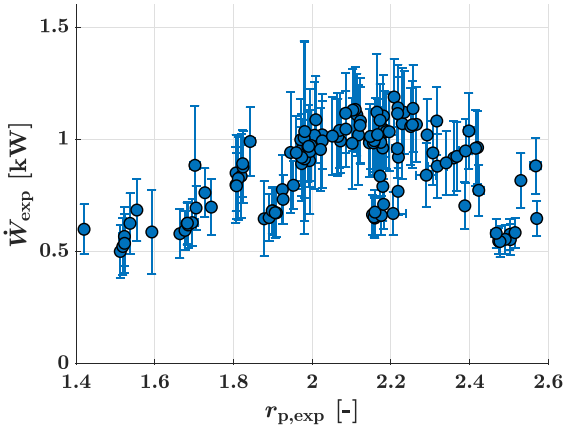

Fig. 11. Expander output power as a function of the expander pressure ratio.

($\dot{W}_{net}/\dot{W}_{eng}$) is plotted against the ratio of the extracted heat and the available heat ($\dot{Q}_{evap}/\dot{Q}_{cool}$) for the different engine operating points. The relative power clearly increased with the relative heat transfer rate, indicating that the system performance was mainly limited by its ability to extract heat from the coolant. Only at one operating point (A25), the maximum pump speed (and thus mass flow) was limited by the available heat in the coolant rather than the pressure fluctuations. At this operating point (the blue marker in the upper right corner in Fig. 15) the WHR system extracted almost 60% of the available heat, giving a net relative power of more than 0.7%. The pressure fluctuations significantly impacted the system performance because it was unable to operate at the performance level it was designed for; clearly visible from the maximum pump speed of 450 rpm (of the available 1450 rpm) and the maximum evaporator heat load of 50 kW (of the available 125 kW).

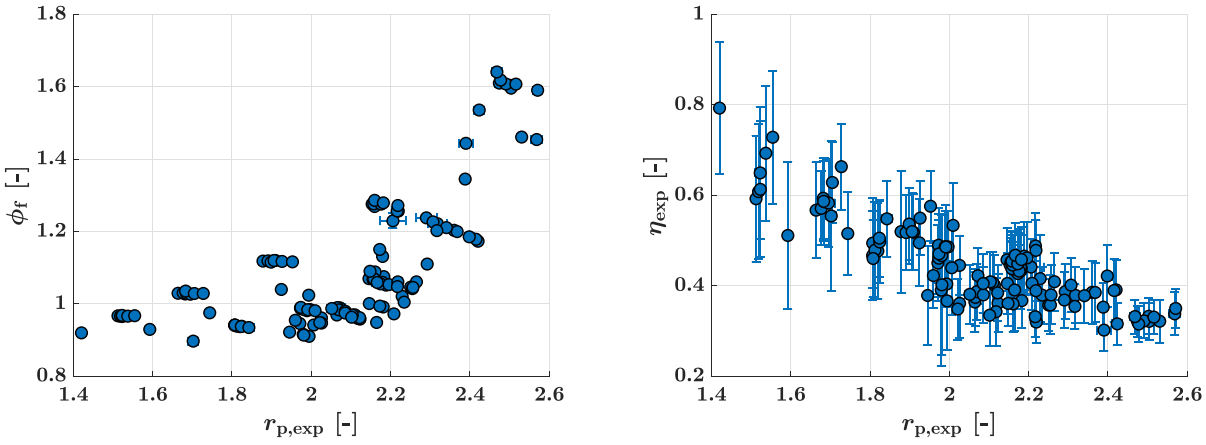

Fig. 12. Expander filling factor (left) and efficiency (right) as functions of the expander pressure ratio.

Table 8
Expander specifications [37,38].

Brand	GAST 6AM-FRV-5A	
Type	Sliding vane	
Max. speed	N_{exp}	3000 rpm
Max. volume flow	$\dot{V}_{exp}$	3750 L/min
Eccentricity	e	5 mm
Diameter of cylinder bore	D	82 mm
Number of vanes	m	4
Vane thickness	s	4 mm
Cylinder length	L	63 mm
Displacement	V_{exp}	0.152 L

Table 9
Condenser specifications [36].

Brand	SWEP B250ASHx60	
Type	Plate, counter-current	
Max. pressure drop	Δp_{cond}	4.94 kPa
Max. heat load	$\dot{Q}_{cond}$	116 kW

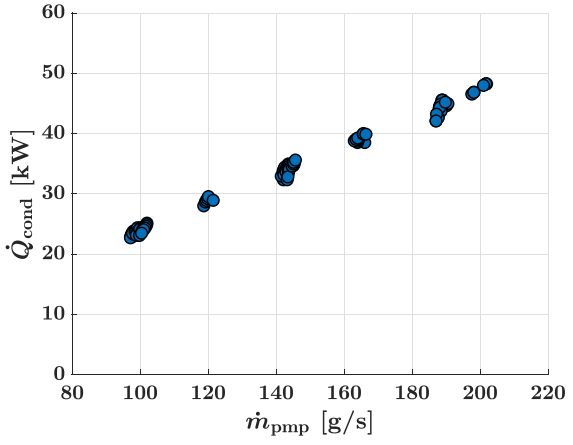

Fig. 13. Condenser heat transfer rate as a function of the mass flow.

3.7. Condensation pressure

The condensation pressure is an important parameter of a LT-WHR system because it directly determines the condensation temperature and thus the temperature at which the heat is rejected. The condensation pressure in the system was varied by regulating the air pressure in the expansion tank while maintaining a constant expander inlet pressure, effectively changing the pressure ratio. The effect of varying the condenser inlet pressure ($p_{cond,in}$) on the condensation temperature ($T_{sat,cond}$) and net power ($\dot{W}_{net}$) is shown in Fig. 16 for a selection of engine operating points. As expected, increasing the condensation pressure increased the condensation temperature and therefore allows for enhanced heat transfer to the ambient. However, the net power output decreased because the expander pressure ratio decreased.

3.8. Coolant temperature

The effect of the engine coolant temperature on the cycle performance was studied by increasing the temperature of the coolant entering the engine, thereby effectively increasing the engine coolant outlet temperature. The engine coolant outlet temperature was increased from its normal operating value of 92 °C to 107 °C in steps of 5 °C. During these experiments, the pump speed was kept constant, while the expander speed was varied between 1500 and 2100 rpm. The resulting net power output for the different coolant temperatures is shown on the left of Fig. 17. Increasing the coolant temperature had significant effects, increasing the net power by almost 30% in some cases. Another positive effect is shown on the right of Fig. 17, which shows the corresponding pressure ratios at the same expander speeds and coolant temperatures. Since the pressure ratio increased at elevated coolant temperatures, the condensation pressure ratio could be increased. Although this would reduce power output, it would increase the condensation temperature, allowing for better heat rejection to the ambient. In this study, the coolant temperature was limited to 107 °C, but even higher coolant temperatures (> 120 °C), could lead to considerable gains for the WHR system in terms of net power or condensation temperature.

4. Cycle Model

The modeling of cycle components may be broadly classified into three approaches: empirical, semi-empirical, and deterministic [40]. Empirical models are based on expressions with selected variables that were fitted on experimental results, whereas semi-empirical include physical relations calibrated using the experimental results. Deterministic models are based on the equations of mass, momentum, and energy to give a comprehensive description of the physical processes. Because of the physical basis of semi-empirical and deterministic models, they provide a deeper insight into the physical phenomena that occur and allow for simulating the system outside the experimental range. However, this involves a more elaborate modeling approach and is typically associated with higher computational costs [40]. In this study, the

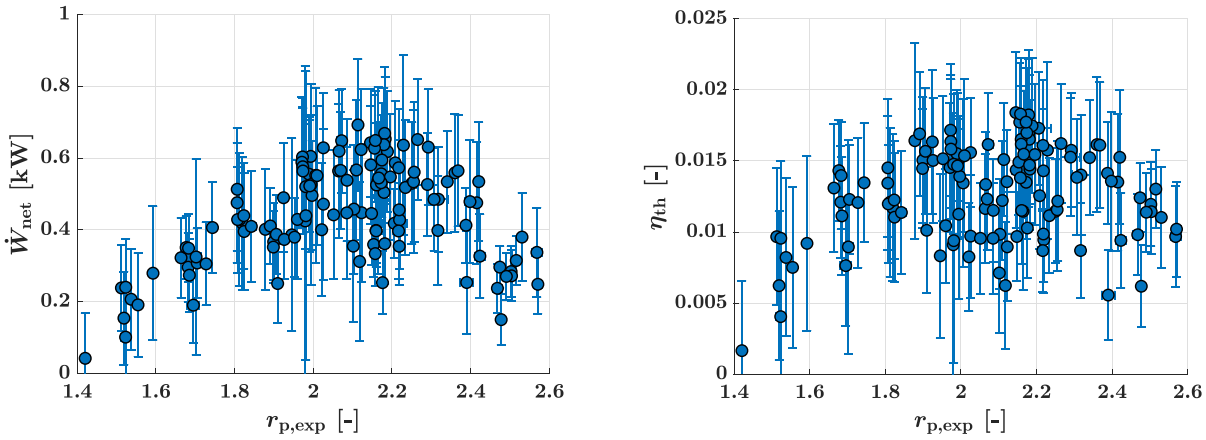

Fig. 14. Net cycle power (left) and thermodynamic efficiency (right) as functions of the expander pressure ratio.

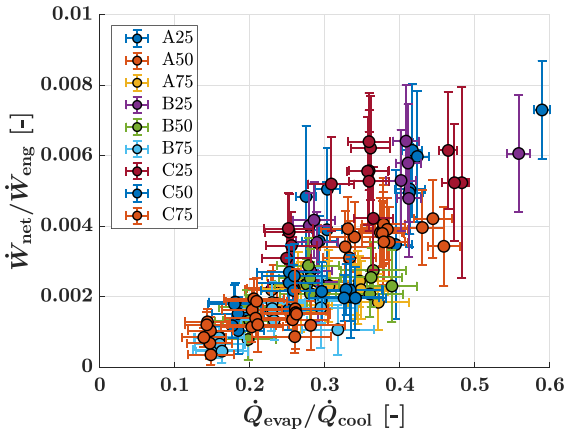

Fig. 15. Relative power output as a function of the heat transfer capacity.

experimental results were used as the basis for a steady-state empirical model that is depicted schematically in Fig. 18. Although the empirical model presented here is based on relatively few variables, the model allows for an initial evaluation of the performance of this system in a driving cycle, which can serve as a baseline for further study. The coolant flow and temperature are used as inputs and four main components were modeled: the pump, evaporator, expander, and condenser.

The pump flow fit in Eq. (3) is based on manufacturer data [35]. The volume flow ($\dot{V}_{pmp}$, in L/min) depends on the pump speed (N_{pmp}, in rpm) and is corrected for the outlet pressure ($p_{pmp,out}$, in bar).

$$\dot{V}_{pmp} = 0.022N_{pmp} - (0.001N_{pmp} - 0.1)\frac{p_{pmp,out}}{69} \tag{3}$$

The efficiency curve of the pump is based on published experimental data for this pump [7] and depends on the pressure change. The pump flow fit and the efficiency curve are shown in Fig. 19. The efficiency of the pump was determined using linear interpolation between the data points shown in the figure, where the pump pressure change was used as input.

The heat exchangers are modeled as simple heat transfer devices with an effectiveness of 1 (i.e., assuming no external heat losses) and a pinch point temperature difference of 4 K. The performance of the expander is determined by its filling factor (ϕ_f), efficiency (η_{exp}), and isentropic effectiveness (ϵ_{is}), as defined in Eq. (8), (9), and (10). To obtain relations for these three performance factors, a simple fit based on the pressure ratio was defined, as shown in Eq. ()()()(4)–(6).

$$\phi_f = \max\left(0.95, \frac{2.6 \cdot r_{p,exp}}{7}\right) \tag{4}$$

$$\eta_{exp} = \min\left(0.7, \frac{1}{3.5 \cdot \ln(r_{p,exp})}\right) \tag{5}$$

$$\epsilon_{is} = \max\left(0.5, \eta_{exp}\right) \tag{6}$$

To study the effect of the expander performance, an optimized expander fit was also defined by increasing the values for the standard fit

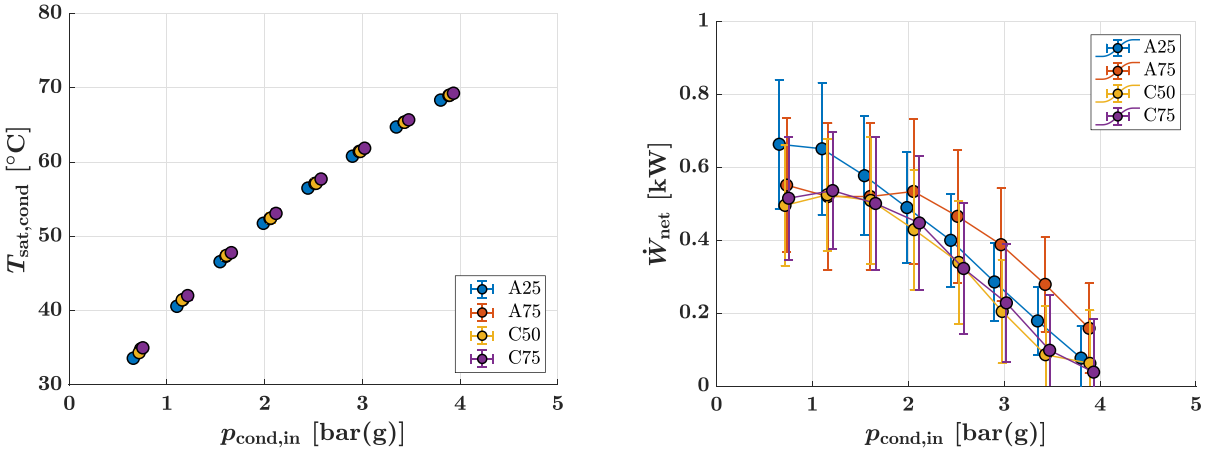

Fig. 16. Condensation temperature (left) and net cycle power (right) as functions of the condensation pressure for selected engine operating points.

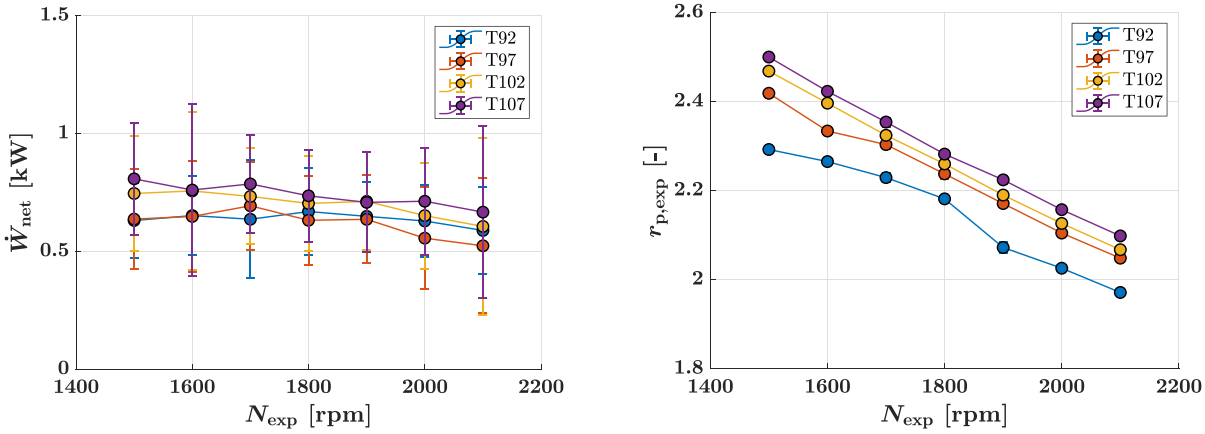

Fig. 17. Net cycle power (left) and expander pressure ratio as functions of the expander speed for different engine coolant temperatures.

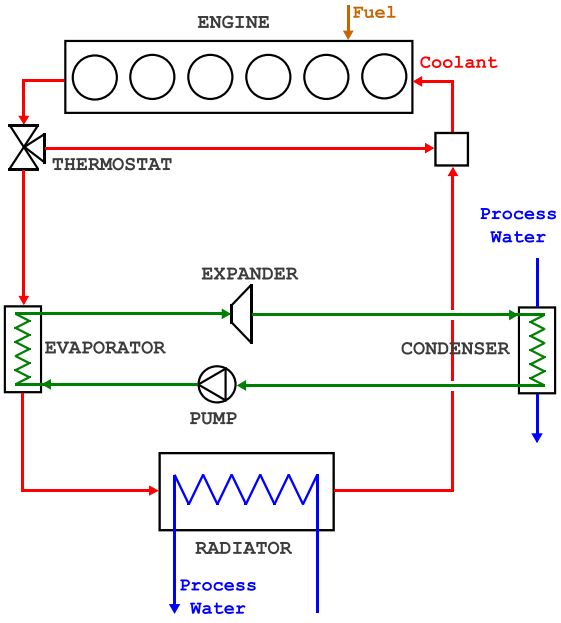

Fig. 18. Schematic depiction of the LT-WHR model.

while maintaining the original profile, mathematically expressed as:

$$\eta_{exp,opt} = \min\left(0.8, \frac{1}{2.5 \cdot \ln(r_{p,exp})}\right) \quad (7)$$

The resulting fits and the corresponding experimental data are visualized in Fig. 20.

The models described above were implemented in MATLAB [31]. The fluid properties were taken from fluid maps generated using data from the CoolProp database [32]. Using a constrained optimization routine (fmincon) the mass flow of the pump and expander were matched by varying the pump outlet pressure. A golden section search was employed to find the expander speed that gave the highest net power. Fig. 21 compares the experimental and the model values for the previously shown experimental results. The good fit for the expander inlet temperature ($T_{exp,in}$), expander inlet pressure ($p_{exp,in}$), and pump mass flow ($\dot{m}_{pmp}$) indicate that the simplified models of the pump, heat exchangers, and expander filling factor provide good estimates. As expected, the expander power ($\dot{W}_{exp}$) is not solely dependent on the pressure ratio, causing the model to deviate from the experimental values. Nevertheless, the performance estimates are good enough to use in simulations.

To evaluate the performance of the LT-WHR system, the radiator mass flows and inlet temperatures during a long haul driving cycle are used as input, which are shown in Fig. 22.

To reduce computational cost, the range of inlet conditions was divided into a four by four grid. This grid is shown in Fig. 23 with the relative time spent in each operating point during the driving cycle. Simulations were performed for each center-point. The performance was

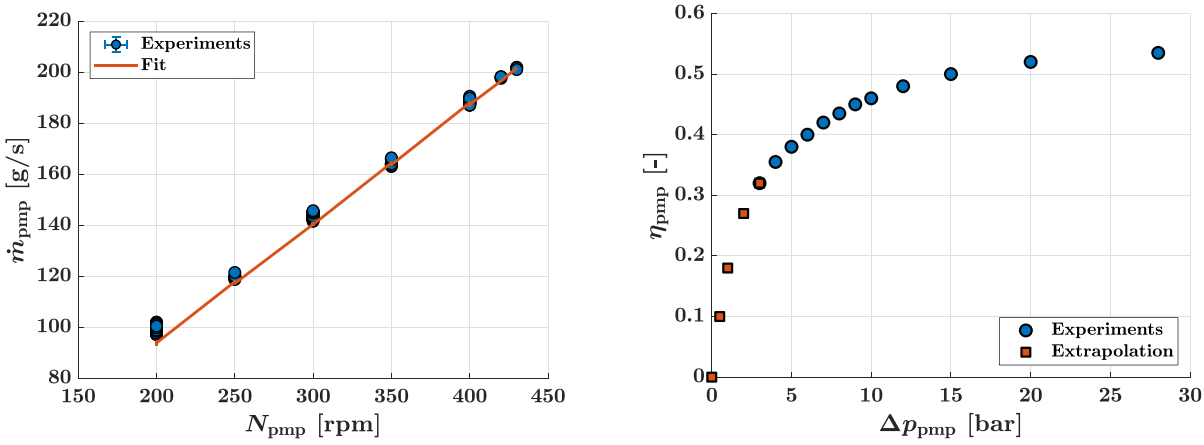

Fig. 19. Pump mass flow (left) and its estimated efficiency curve [7] (right).

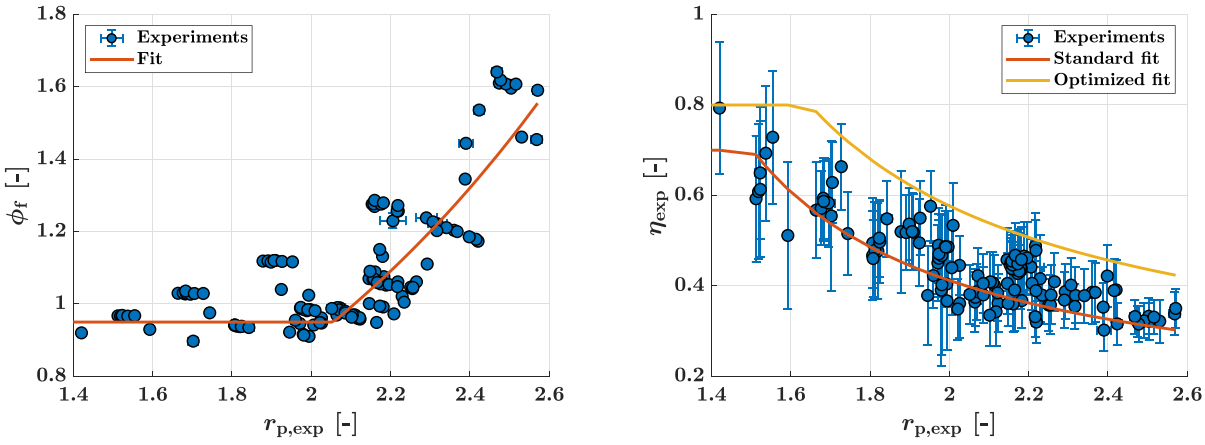

Fig. 20. Expander filling factor (left) and efficiency (right).

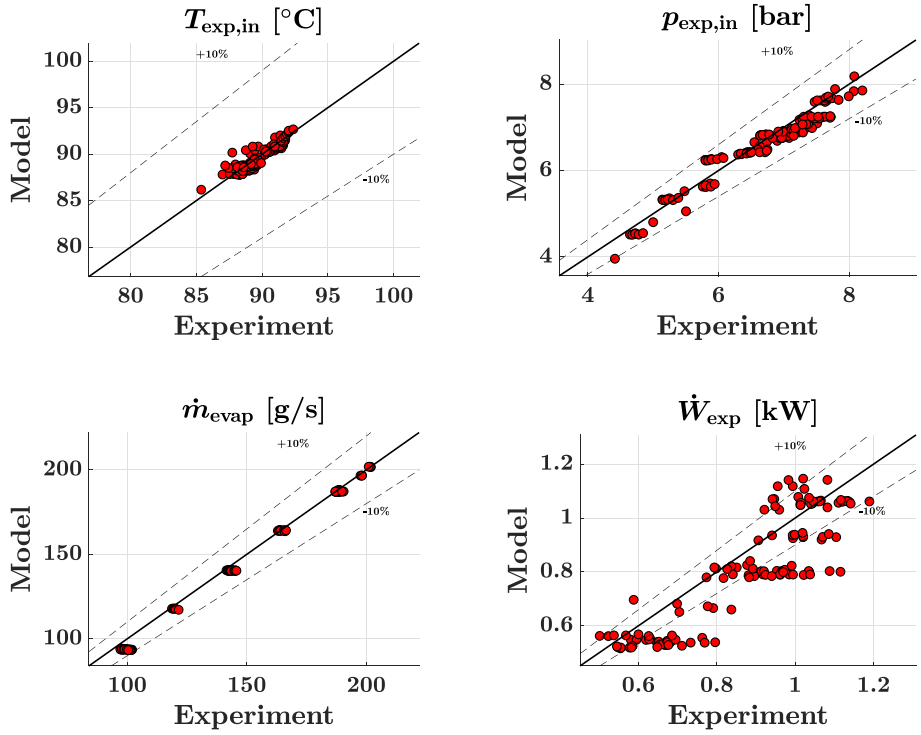

Fig. 21. Comparison of experimental and model results.

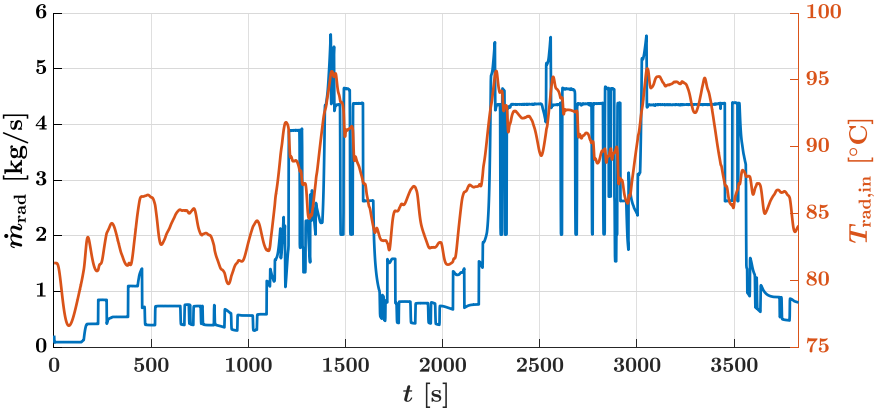

Fig. 22. Radiator mass flow rate and inlet temperature for a representative driving cycle for a long haul truck on an European road.

estimated with using Eq. (5) and (9). At positive engine torque (τ_{eng}) the expander power is directly provided to the engine, while at negative engine torque the expander power is converted into electrical power.

$$\dot{W}_{pmp,el} = \frac{\dot{W}_{pmp}}{\eta_{el}} \tag{8}$$

$$\dot{W}_{exp} = \begin{cases} \dot{W}_{exp,mech} = \eta_{mech}\dot{W}_{exp}, & \text{if } \tau_{eng} > 0 \\ \dot{W}_{exp,el} = \eta_{el}\dot{W}_{exp}, & \text{if } \tau_{eng} \leqslant 0 \end{cases} \tag{9}$$

The mechanical and electrical efficiencies and the other constant model parameters are summarized in Table 10, together with the constraints used in the model.

5. Modeling Results

The previously described 16 operating points were used as inputs for the low-temperature cycle simulations whose results are shown in Table 11. Two systems were simulated: the standard system, which uses a variable pump efficiency (η_{pmp}), as shown in Fig. 19, and uses the standard expander fit (η_{exp}), as shown in Fig. 20. Additionally, an optimum system was defined, where the pump efficiency was set to a constant high value of 0.5 and the optimized expander fit ($\eta_{exp,opt}$) was used, also shown in Fig. 20. The results clearly show that there is not much difference between the two systems apart from the net power output ($\dot{W}_{net}$) and thermodynamic efficiency (η_{th}). Since the heat extraction from the engine coolant is similar for both systems but the net power output of the optimum system is higher, the optimum system has a higher thermodynamic efficiency.

Based on the results of the simulations, performance maps of both systems were generated covering the full operational range of simulated engine operating points. The map for the standard system is shown on left of Fig. 24 and that for the optimum system on the right. The maps indicate that increasing the pump and expander efficiency can improve system performance by over 50%.

The net power output during the driving cycle was determined using the performance maps, as shown in Fig. 25. The values shown in Fig. 22 were used as inputs. Transient effects were not taken into account; if included, they would mainly dampen the temperature (but not the mass flow) fluctuations in the evaporator. The expander was allowed to run at its optimum speed over the whole driving cycle. In practical applications, the expander speed would be determined by the engine speed (and a gear ratio) when it is mechanically coupled to the engine. In addition to the standard and optimum systems, results are shown using the standard fit for the expander efficiency with a fixed pump efficiency of 0.5.

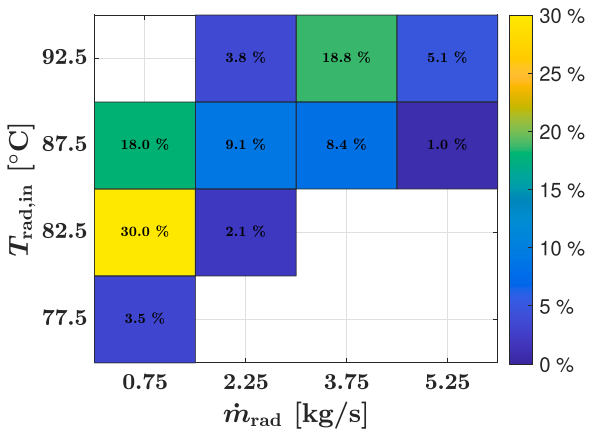

Fig. 23. Relative time distributions of the different inlet conditions (radiator mass flows and inlet temperatures) for the driving cycle. The total drive cycle time (Δt_{dc}) is 3832 s.

Table 10
Cycle inputs and constraints.

Inputs			
Condensation pressure	p_{cond}	3	bar
Condensation temperature	T_{cond}	51	°C
Pump inlet subcooling temperature	ΔT_{sub}	5	K
Pinch point temperature difference	ΔT_{pp}	4	K
Heat exchanger effectiveness	ϵ	1	-
Electrical generator efficiency	η_{el}	0.85	-
Mechanical coupling efficiency	η_{mech}	0.98	-
Constraints			
Evaporator outlet superheating temp.	ΔT_{sup}	>2	K
Expander speed	N_{exp}	200–3000	rpm
Pump speed	N_{pmp}	100–1450	rpm

The net power output is the difference between the power consumed by the pump and that produced by the expander. The expander power depends on the expander efficiency and the amount of heat extracted from the heat source. In the simulations, the upper limit for heat extraction was equal to the heat that was normally rejected by the radiator during the driving cycle ($\dot{Q}_{tot}$), computed using Eq. (10).

$$\dot{Q}_{tot} = \dot{Q}_{rad} + \dot{Q}_{cond} \tag{10}$$

Since the WHR system takes the heat from the engine coolant, the heat that is extracted does not need to be cooled in the radiator anymore. The heat transfer rates for the condenser and the radiator during the driving cycle are shown in Fig. 26. The figure shows that most of the coolant heat is transferred to the LT-WHR system and in certain intervals the radiator is not used at all.

The results for the driving cycle can be integrated over time to evaluate the total energy recovered by the WHR system over the whole driving cycle, as shown in Table 12. As is also visible from Fig. 26, the integrated results indicate that most of the heat is rejected by the condenser (91.5%). No significant effect on the heat transfer rate in the evaporator is visible for the different systems. The total net recovered energy for the standard system was 2.96 MJ, which corresponds to 0.73% of the work done by the engine, which roughly translates to an equal reduction in fuel consumption. With a more efficient pump, this could be improved to 0.87%. Improving the expander efficiency increased the recovered energy even further to 1.29% relative to the engine work. When the results from the driving cycle are compared to the relative power improvements in Table 1, it is visible that the performance of the WHR system in this study is much lower than the presented systems. This is partly because in the existing literature almost all studies were taking multiple heat sources into account. Furthermore, the setup under investigation in this paper can be optimized to improve its performance. However, simulations tend to overestimate efficiencies and underestimate losses, which is reflected in the difference in results. This study shows that for a realistic evaluation of the system performance, pump and expander performance, system losses, and heat transfer to and from the system, must be carefully considered.

6. Discussion

- The fluctuations of the pump inlet pressure and the expander torque, shown in Fig. 27, made it impossible to use the full capacity of the WHR system. These fluctuations could have been caused by air in the system or cavitation in the pump resulting from low suction pressure or pipes with insufficiently large diameters.
- In the experimental results shown in this paper, the working fluid was condensed using process water from the test cell. However, in a real truck this heat would have to be rejected through a separate

Table 11
Range of cycle conditions for the 16 operating points.

	$\dot{m}_{pmp}$ g/s	p_{evap} rpm	$T_{exp,in}$ bar	N_{exp} °C	$\dot{Q}_{cond}$ kW	$\dot{W}_{net}$ kW	η_{th} %	η_{exp} %
Standard	145–440	4.4–7.4	70–88	2688–3000	27.9–88.1	0.5–1.7	1.8–2.0	32–70
Optimum	160–440	4.3–7.4	69–88	3000	30.5–88.1	0.8–2.9	2.5–3.5	45–80

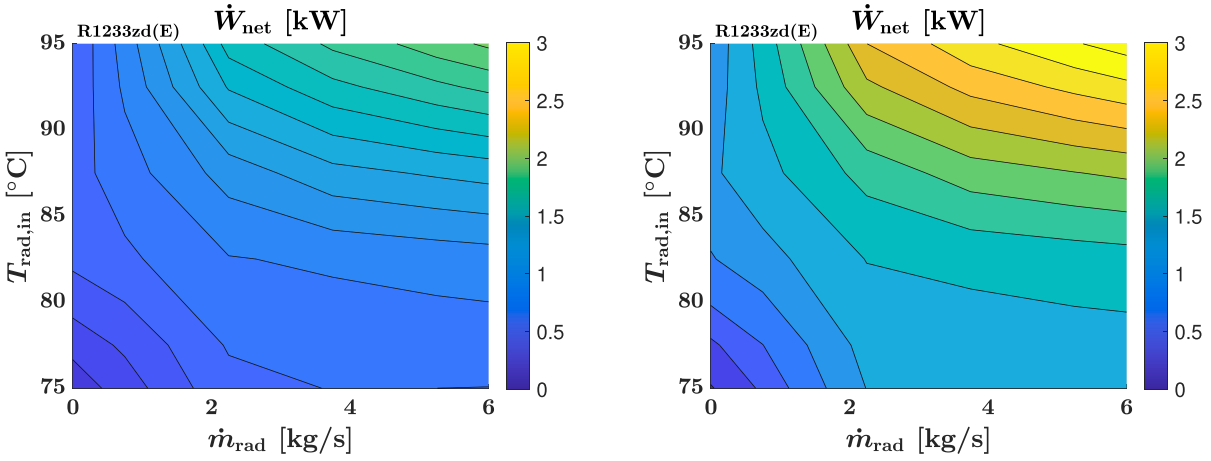

Fig. 24. Net shaft power for the standard (left) and optimum (right) system as functions of the radiator mass flow and inlet temperature. The values at the edges were linearly extrapolated.

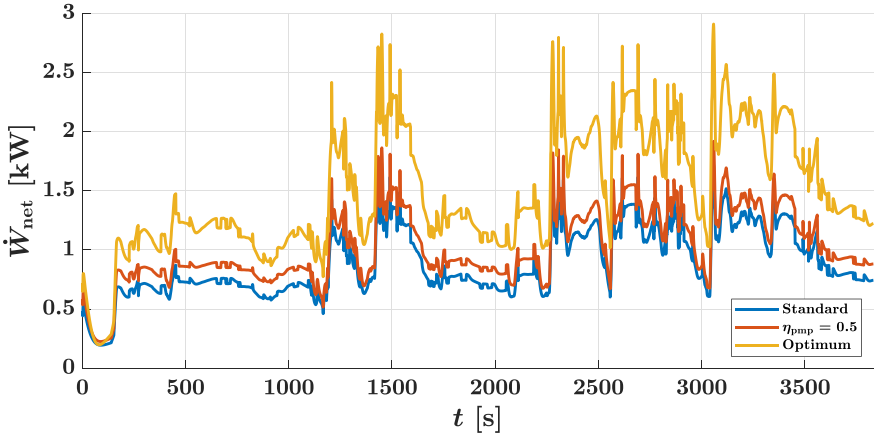

Fig. 25. Net shaft power for three LT-WHR systems during the driving cycle.

radiator (direct condensation) or an intermediate loop (indirect condensation). The lower temperature for heat rejection may necessitate additional power from an existing or additional cooling fan, which would reduce the performance benefit of the WHR system [9].

- The effect of the oil mixed into the working fluid was not taken into account. In the calculations and simulations it was assumed that the flow consisted exclusively of R1233zd(E) even though the working fluid used in the experiments contained a significant amount of oil (∼ 5 mass%).
- The fit for the expander efficiency was not sufficient to accurately predict its power output. A more extensive expander model is thus needed to capture the behavior of the expander. This could be a more sophisticated empirical model or the semi-empirical model from Lemort [41], calibrated with the available experimental data.
- Future simulation studies should focus on the effect of elevated coolant temperatures and condensing pressures. Higher coolant temperatures allow for an increased power output due to an increased pressure ratio in the cycle and could also enhance the heat transfer rate in the evaporator, although the available heat in the engine coolant might decrease because of the reduced heat transfer rates during combustion. Using the engine coolant at elevated temperatures could lead to potential fuel consumption reductions of 4.5% [12]. The effect of raising the condensation pressure should also be studied in more detail because of its importance for heat rejection in automotive applications. An interesting concept is to control the condensation pressure based on the required cooling capacity of the system to optimize the power output [9].
- Finally, the system performance of the WHR system should be studied when integrated in a full vehicle model. In any practical application, a LT-WHR system will be a part of a complete thermal-electric system (including engine, air-conditioning unit, battery, etc.). The interactions between these systems must be properly tuned to optimize overall system performance.

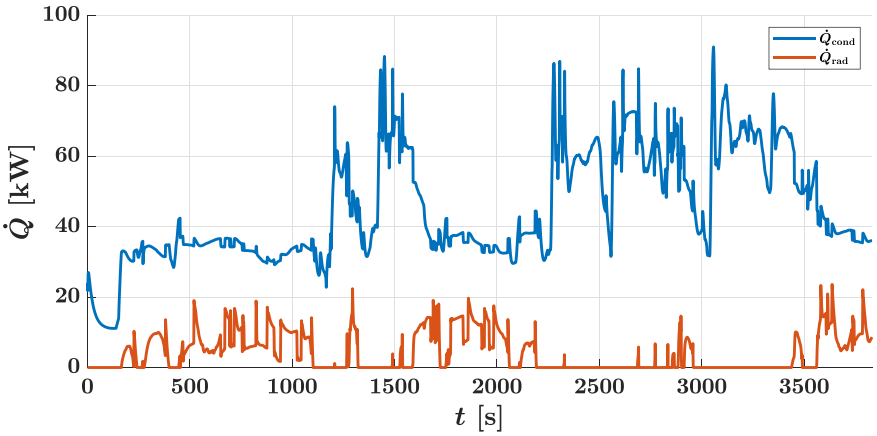

Fig. 26. Condenser and radiator heat transfer rate during the driving cycle for the standard LT-WHR system.

Table 12
Driving cycle performance with a total engine work requirement of 408 MJ.

	Q_{rad} MJ (%)	Q_{cond} MJ (%)	$W_{pmp,el}$ MJ (%)	$W_{exp,mech}$ MJ (%)	$W_{exp,el}$ MJ (%)	W_{net}* MJ (%)
Standard	16 (8.5)	172 (91.5)	1.65 (0.41)	3.99 (0.98)	0.62 (0.15)	2.96 (0.73)
$\eta_{pmp} = 0.5$	16 (8.5)	172 (91.5)	1.05 (0.26)	3.98 (0.98)	0.62 (0.15)	3.55 (0.87)
Optimum	16 (8.5)	172 (91.5)	1.05 (0.26)	5.45 (1.34)	0.84 (0.21)	5.25 (1.29)

* $W_{net} = W_{exp,mech} + W_{exp,el} - W_{pmp,el}$

7. Conclusions

This paper presents the performance of a low-temperature waste heat recovery system coupled to a heavy-duty engine in which R1233zd(E) was used as the working fluid to extract heat from the engine coolant. The aim of this paper is to present the details of the experimental setup and to provide a realistic assessment of the performance of such a system. With the help of simple empirical models, the results were also used to estimate the net recovered power during a long haul driving cycle. Based on the results obtained and the preceding discussion, a number of conclusions can be drawn:

- Although the selected components of the experimental setup were well dimensioned for WHR from the engine coolant of the heavy-duty engine, the WHR system could not be operated at its full capacity for all engine operating points because fluctuations in the pump inlet pressure and the expander torque limited the pump and expander speed. These fluctuations were most likely caused by air in the system or cavitation resulting from insufficient suction pressure or underdimensioned inlet piping for the pump.
- The experimental measurements showed a maximum evaporation pressure of 8 bar, an expander inlet temperature between 88 and 92 °C, and a maximum expander shaft power of 1.2 kW. The expander filling factor ranged between 0.9 and 1.7 and the expander efficiency between 30 and 80%. For a range of engine operating points and using an estimated efficiency for the pump, between 0.1 and 0.7 kW net shaft power was obtained with a thermodynamic efficiency between 1.1 and 1.8%. A maximum of 0.7% of expander power relative to the engine power was achieved.
- The experimental results were used to develop simple empirical cycle models to be able to estimate the performance of the experimental system during a long haul driving cycle. The results suggested that up to 0.7% of the required engine energy could be recovered. Simulations with an increased pump and expander efficiency indicated that it was possible to achieve an energy recovery of 1.3%. More accurate simulations would require the development of a more sophisticated expander model.
- Experiments were performed to evaluate the influence of the condensation pressure and engine coolant temperature on the cycle performance. Increasing the condensation pressure from 1.5 to 5 bar reduced the net power output from 0.7 to 0.1 kW, while raising the coolant temperature from 92 to 107 °C delivered a potential net power increase of 30%. Further simulations are needed to determine

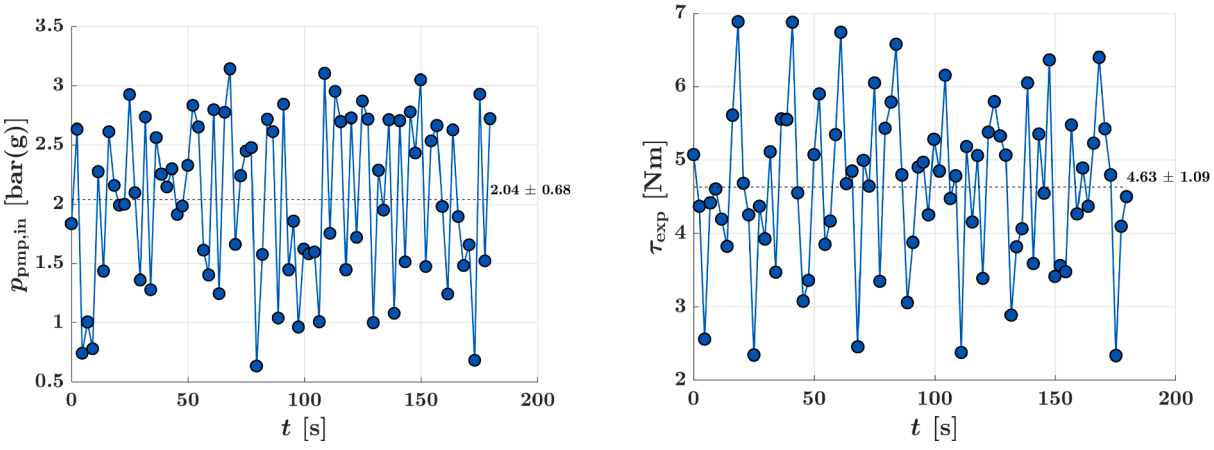

Fig. 27. Fluctuations in the pump inlet pressure (left) and the expander torque (right).

the effect of these conditions on the performance during a long haul driving cycle.

CRediT authorship contribution statement

Jelmer Rijpkema: Conceptualization, Investigation, Methodology, Software, Validation, Writing - original draft. **Sven B. Andersson:** Supervision. **Karin Munch:** Supervision.

Declaration of Competing Interest

The authors declare that they have no known competing financial interests or personal relationships that could have appeared to influence the work reported in this paper.

Acknowledgments

This research was made possible by funding provided by the Strategic Vehicle Research and Innovation Programme (FFI) of the Swedish Energy Agency. The authors would like to thank the partners in the WHR project: Gnutti Carlo, IAV, KTH Royal Institute of Technology, Lund University, Scania, TitanX, Volvo Cars, and Volvo Group. Special thanks go out to Dr. Sasan Sarmast from Gnutti Carlo and Dr. Olof Erlandsson from TitanX for providing hardware and assistance. The help during the design phase from Dr. Olivier Dumont of the University of Liège is also gratefully acknowledged.

References

[1] International Energy Agency, Energy Technology Perspectives 2020. 2020.
[2] Reitz RD, et al. IJER editorial: The future of the internal combustion engine. Int J Engine Res 2019.
[3] Joshi A, "Review of Vehicle Engine Efficiency and Emissions," SAE Technical Paper 2020-01-0352, 2020.
[4] Lion S, Michos CN, Vlaskos I, Rouaud C, Taccani R. A review of waste heat recovery and Organic Rankine Cycles (ORC) in on-off highway vehicle Heavy Duty Diesel Engine applications. Renew Sustain Energy Rev 2017;79.
[5] Su X, Shedd TA. Towards working fluid properties and selection of Rankine cycle based waste heat recovery (WHR) systems for internal combustion engines – A fundamental analysis. Appl Therm Eng 2018;142.
[6] Zhao Y, Liu G, Li L, Yang Q, Tang B, Liu Y. Expansion devices for organic Rankine cycle (ORC) using in low temperature heat recovery: A review. Energy Convers Manage 2019;199.
[7] Guillaume L, Lemort V, "Comparison of different ORC typologies for heavy-duty trucks by means of a thermo-economic optimization," Energy, vol. 182, 2019.
[8] Imran M, Haglind F, Lemort V, Meroni A, "Optimization of organic rankine cycle power systems for waste heat recovery on heavy-duty vehicles considering the performance, cost, mass and volume of the system," Energy, vol. 180, 2019.
[9] Galuppo F, Reiche T, Lemort V, Dufour P, Nadri M. Organic Rankine Cycle based waste heat recovery modeling and control of the low pressure side using direct condensation and dedicated fans. Energy 2020.
[10] Tian H, Zhang C, Li X, Shu G, "Experimental investigation on diesel engine's waste heat capacity under mapping characteristics", Science China Technological Sciences, vol. 58, 2015.
[11] Rijpkema J, Munch K, Andersson SB. Thermodynamic potential of twelve working fluids in Rankine and flash cycles for waste heat recovery in heavy duty diesel engines. Energy 2018;160.
[12] Singh V, Rijpkema J, Li X, Munch K, Andersson S, Verhelst S, "Optimization and Evaluation of a Low Temperature Waste Heat Recovery System for a Heavy Duty Engine over a Transient Cycle," SAE Technical Paper 2020-01-2033, 2020.
[13] Hoang AT. Waste heat recovery from diesel engines based on Organic Rankine Cycle. Appl Energy 2018;231.
[14] Mahmoudi A, Fazli M, Morad MR. A recent review of waste heat recovery by Organic Rankine Cycle. Appl Therm Eng 2018;143.
[15] Xu B, Rathod D, Yebi A, Filipi Z, Onori S, Hoffman M. A comprehensive review of organic rankine cycle waste heat recovery systems in heavy-duty diesel engine applications. Renew Sustain Energy Rev 2019;107.
[16] Mondejar ME, Andreasen JG, Pierobon L, Larsen U, Thern M, Haglind F. A review of the use of organic Rankine cycle power systems for maritime applications. Renew Sustain Energy Rev 2018;91.
[17] Scaccabarozzi R, Tavano M, Invernizzi CM, Martelli E. Comparison of working fluids and cycle optimization for heat recovery ORCs from large internal combustion engines. Energy 2018;158.
[18] Yu G, Shu G, Tian H, Wei H, Liu L. Simulation and thermodynamic analysis of a bottoming Organic Rankine Cycle (ORC) of diesel engine (DE). Energy 2013;51.
[19] Yang K, Zhang H, Song S, Zhang J, Wu Y, Zhang Y, et al., "Performance Analysis of the Vehicle Diesel Engine-ORC Combined System Based on a Screw Expander," Energies, vol. 7, 2014.
[20] Araya S, Wemhoff AP, Jones GF, Fleischer AS, "An experimental study of an Organic Rankine Cycle utilizing HCFO-1233zd(E) as a drop-in replacement for HFC-245fa for ultra-low-grade waste heat recovery," Applied Thermal Engineering, vol. 180, 2020.
[21] Eyerer S, Dawo F, Kaindl J, Wieland C, Spliethoff H. Experimental investigation of modern ORC working fluids R1224yd(Z) and R1233zd(E) as replacements for R245fa. Appl Energy 2019;240.
[22] Rijpkema J, Andersson S, Munch K, "Thermodynamic Cycle and Working Fluid Selection for Waste Heat Recovery in a Heavy Duty Diesel Engine," SAE Technical Paper 2018-01-1371, 2018.
[23] Peris B, Navarro-Esbrí J, Molés F. Bottoming organic Rankine cycle configurations to increase Internal Combustion Engines power output from cooling water waste heat recovery. Appl Therm Eng 2013;61.
[24] Mashadi B, Kakaee A, Jafari Horestani A, "Low-temperature Rankine cycle to increase waste heat recovery from the internal combustion engine cooling system," Energy Conversion and Management, vol. 182, 2019.
[25] Furukawa T, Nakamura M, Machida K, Shimokawa K, "A Study of the Rankine Cycle Generating System for Heavy Duty HV Trucks," Apr 2014.
[26] Shu G, Yu G, Tian H, Wei H, Liang X, Huang Z. Multi-approach evaluations of a cascade-Organic Rankine Cycle (C-ORC) system driven by diesel engine waste heat: Part A - Thermodynamic evaluations. Energy Convers Manage 2016;108.
[27] Chen T, Zhuge W, Zhang Y, Zhang L, "A novel cascade organic Rankine cycle (ORC) system for waste heat recovery of truck diesel engines," Energy Conversion and Management, vol. 138, 2017.
[28] Liu P, Shu G, Tian H, Wang X, Yu Z. Alkanes based two-stage expansion with interheating Organic Rankine cycle for multi-waste heat recovery of truck diesel engine. Energy Mar 2018;147.
[29] Rijpkema J, Munch K, Andersson SB. Combining Low- and High-Temperature Heat Sources in a Heavy Duty Diesel Engine for Maximum Waste Heat Recovery Using Rankine and Flash Cycles. In: Junior C, Dingel O, editors. Energy and Thermal Management, Air-Conditioning, and Waste Heat Utilization. Springer International Publishing; 2019.
[30] Thantla S, Aspfors J, Fridh J, Erlandsson AC. characterization of an organic rankine cycle system for waste heat recovery from heavy-duty engine coolant and exhaust. In: Proceedings of the 5th International Seminar on ORC Power Systems; 2019.
[31] MathWorks, MATLAB, Version R2019a, 2019.
[32] Bell IH, Wronski J, Quoilin S, Lemort V, "Pure and pseudo-pure fluid thermophysical property evaluation and the open-source thermophysical property library CoolProp," Industrial and Engineering Chemistry Research, vol. 53, no. 6, 2014.
[33] Taylor J. An Introduction to Error Analysis: The Study of Uncertainties in Physical Measurements. University Science Books; 1997.
[34] "DieselNet: Emission test cycles - European Stationary Cycle (ESC)." url:https://www.dieselnet.com/standards/cycles/esc.php. Accessed: 2021-01-04.
[35] "Wanner Hydra-Cell. G10 Pump Datasheet." Accessed: 2020-12-23.
[36] "SWEP. SSP G8 Calculation Software v2020.825.2." Accessed: 2020-04-19.
[37] "GAST. Product Specifications 6AM-FRV-5A." Accessed: 2020–12-23.
[38] Daminabo FFO, A novel 2kWe Biomass-Organic Rankine Cycle Micro Cogeneration System. PhD thesis, 2009.
[39] Brown RN. Compressors: Selection and Sizing. Elsevier; 2005.
[40] Lemort V, Guillaume L, Declaye S, Quoilin, S "A comparison of piston, screw and scroll expanders for small scale Rankine cycle systems," Proceedings of the 3rd international conference on microgeneration and related technologies., 2013.
[41] Lemort V, Contribution To the Characterization of Scroll Machines in Compressor and Expander Modes. PhD thesis, 2008.